AMERICAN SOCIETY FOR MICROBIOLOGY | Applied and Environmental Microbiology

The Siderophore Metabolome of *Azotobacter vinelandii*

Oliver Baars,[a] Xinning Zhang,[a] François M. M. Morel,[a] Mohammad R. Seyedsayamdost[b]

Department of Geosciences[a] and Department of Chemistry,[b] Princeton University, Princeton, New Jersey, USA

In this study, we performed a detailed characterization of the siderophore metabolome, or "chelome," of the agriculturally important and widely studied model organism *Azotobacter vinelandii*. Using a new high-resolution liquid chromatography-mass spectrometry (LC-MS) approach, we found over 35 metal-binding secondary metabolites, indicative of a vast chelome in *A. vinelandii*. These include vibrioferrin, a siderophore previously observed only in marine bacteria. Quantitative analyses of siderophore production during diazotrophic growth with different sources and availabilities of Fe showed that, under all tested conditions, vibrioferrin was present at the highest concentration of all siderophores and suggested new roles for vibrioferrin in the soil environment. Bioinformatic searches confirmed the capacity for vibrioferrin production in *Azotobacter* spp. and other bacteria spanning multiple phyla, habitats, and lifestyles. Moreover, our studies revealed a large number of previously unreported derivatives of all known *A. vinelandii* siderophores and rationalized their origins based on genomic analyses, with implications for siderophore diversity and evolution. Together, these insights provide clues as to why *A. vinelandii* harbors multiple siderophore biosynthesis gene clusters. Coupled with the growing evidence for alternative functions of siderophores, the vast chelome in *A. vinelandii* may be explained by multiple, disparate evolutionary pressures that act on siderophore production.

Azotobacter vinelandii is a widespread nitrogen-fixing soil bacterium belonging to the *Gammaproteobacteria*. It is an established, genetically tractable model organism for studies of nitrogen fixation and siderophore production (1). Siderophores are Fe-chelating molecules that change the speciation of Fe in the extracellular medium by outcompeting other natural ligands (2). Uptake of the resulting Fe-siderophore complex via membrane-bound receptors allows *A. vinelandii* to gain access to otherwise sparingly soluble Fe (3–5). The Fe-siderophore complexes may be unavailable to competing organisms and thus may exhibit growth-inhibitory or antiphytopathogenic activities (6, 7). Several studies have shown that the siderophores of *A. vinelandii* can also bind metals other than Fe to enable uptake of additional metals required in nitrogenases (Mo, V) (4, 8) or to sequester toxic heavy metals (e.g., W, Zn) (9–11). The siderophores secreted by *A. vinelandii* have also been found to support the growth of some freshwater algae in coculture by providing a significant source of nitrogen to these organisms (12).

The known siderophores of *A. vinelandii* include the fluorescent compounds azotobactin D and azotobactin δ (13, 14) and the catechol siderophores azotochelin (15), aminochelin (16), and protochelin (3). These five siderophores have been discovered and characterized over a span of about 30 years using primarily chemical assays (17), which allow the analysis of only one or a few siderophores at the same time due to limited sensitivity and separation power. Thus, it is possible that *A. vinelandii* produces other, yet-unidentified siderophores.

A recent development in the discovery of siderophores is the use of high-resolution liquid-chromatography electrospray ionization mass spectrometry (HR-LC-MS) methods that exploit the characteristic ^{54}Fe-^{56}Fe isotope pattern associated with organic Fe chelates (18–20). Data mining techniques are available for filtering the relevant Fe isotope patterns associated with Fe complexes even at low abundances and in highly complex matrixes, as well as for detecting the corresponding apo siderophores (18). Characterization of the species thus discovered can then be achieved by analysis of tandem MS (MS/MS) spectra and additional spectroscopic data (e.g., UV-visible [UV-vis] and nuclear magnetic resonance [NMR]).

Parallel to Fe detection approaches, our understanding of siderophore biosynthesis has increased immensely over the last decade to the extent that bioinformatic mining of genomes can reveal gene clusters responsible for siderophore production, although the exact chemical structure of the final products is often difficult to predict (21–23). Nonribosomal peptide synthetase (NRPS) genes involved in the production of the known azotobactin and catechol siderophores have been identified in *A. vinelandii* (24, 25).

In this study, we have combined bioinformatic analyses with untargeted HR-LC-MS to discover siderophores and their biosynthetic gene clusters in *A. vinelandii*. The results provide a number of new insights. The α-hydroxycarboxylate siderophore vibrioferrin was observed in a terrestrial organism and detected at higher concentrations than any of the other siderophores. In addition, a large number of new derivatives of vibrioferrin, azotobactin, and the catechol siderophores, some of which we assign by MS/MS spectral networking methods, have been identified. Finally, functional studies provide insights into possible roles of these siderophores, which begin to explain why *A. vinelandii* carries multiple siderophore biosynthetic gene clusters.

Received 29 September 2015 **Accepted** 2 October 2015

Accepted manuscript posted online 9 October 2015

Citation Baars O, Zhang X, Morel FMM, Seyedsayamdost MR. 2016. The siderophore metabolome of *Azotobacter vinelandii*. Appl Environ Microbiol 82:27–39. doi:10.1128/AEM.03160-15.

Editor: M. Kivisaar

Address correspondence to François M. M. Morel, morel@princeton.edu, or Mohammad R. Seyedsayamdost, mrseyed@princeton.edu.

Supplemental material for this article may be found at http://dx.doi.org/10.1128/AEM.03160-15.

MATERIALS AND METHODS

Bacterial cultures. Batch cultures of wild-type *A. vinelandii* strain CA (also known as strain OP and ATCC 13705) were grown aerobically in a modified Burk's medium ([glucose] = 10 g liter^{-1}; [mannitol] = 10 g liter^{-1}; [KH_2PO_4] = 5 mM; [K_2HPO_4] = 2.3 mM; [$CaCl_2$] = 0.68 mM; [$MgSO_4$] = 0.41 mM; pH 6.7) under diazotrophic, Fe-limiting conditions by shaking at room temperature (8). Fe bioavailability was controlled by the addition of 100 μM EDTA and 0.1 μM $FeCl_3$ in HR-LC-MS experiments. Mo concentration ([Na_2MoO_4] = 1 μM) was higher than required for optimal growth. Other trace metals were supplemented at optimal concentrations ([$CuCl_2$] = 10^{-8} M; [$MnCl_2$] = 2.25×10^{-7} M; [$CoCl_2$] = 2.43×10^{-8} M; [$ZnSO_4$] = 5.3×10^{-8} M) (8). To study the effect of Fe sources, Fe was added as (i) 100 μM EDTA and 0.1 μM $FeCl_3$, (ii) 100 μM EDTA and 5 μM $FeCl_3$, (iii) hematite, and (iv) freshly precipitated Fe oxides. Other medium components remained the same as previously described. Bacterial growth was monitored by measuring optical density at 620 nm (OD_{620}).

Genome mining. The genome of *A. vinelandii* strain CA (GenBank accession number CP005094) was analyzed for siderophores using the secondary metabolite genome mining software AntiSmash (26), the gene annotation software RAST (27), and targeted BLAST homology analyses. The results were compared to those of previously published studies on siderophore synthesis in *A. vinelandii* (24, 25). A concatenated amino acid sequence corresponding to the entire PvsABCDE cluster in *A. vinelandii* was used for vibrioferrin gene discovery in other publicly available genomes based on a tBLASTn search of the NCBI database.

HR-LC-MS and siderophore metabolomic analyses. (i) Sample preparation. For untargeted siderophore profiling, stationary-phase cultures were first collected by centrifugation. The supernatant was filtered, first with a 0.22-μm filter and then with a 3-kDa-cutoff Amicon Ultra ultrafiltration device. Trifluoroacetic acid (TFA) was added to a final concentration of 0.03% (vol/vol) before solid-phase extraction (SPE). After loading, the column (Oasis HLB, 200 mg; Waters) was washed with TFA (0.03% in water) and then formic acid (FA; 0.03% in water), followed by elution with 50% and 100% methanol (MeOH) in water. For further analyses, the two extract fractions were combined. Sterile culture medium was extracted in the same way and used as a blank. Biological control samples extracted under oxygen-free conditions in an anaerobic glove box (Coy chamber) were harvested during early growth (OD_{620} = 0.10). Oxygen concentrations in the culture medium were near the detection limit (0.01 to 0.02 mg liter^{-1} with a Hach HQ40d oxygen electrode) before extraction. Solvents used for these anaerobic extractions were degassed to reach oxygen levels below the detection limit. A control sample was extracted in the same way as described above, and another control sample was extracted without the TFA or FA additions, at neutral pH. Concentrated methanolic extracts were dried in a SpeedVac (ThermoFisher) and reconstituted with aqueous mobile-phase buffer prior to LC-MS analyses.

(ii) HR-LC-MS measurement. HR-LC-MS analyses were performed on a high mass accuracy and resolution, reversed-phase high-pressure liquid chromatography (HPLC)-MS platform, using a C_{18} column (ACE 3 C_{18}-AR, 1 mm by 10 cm; MAC-MOD) coupled to an LTQ-Orbitrap XL hybrid mass spectrometer (ThermoFisher). Injected samples (5 μl) were separated (1 h) under a gradient of solutions A and B (solution A consisted of water, 0.1% FA, and 0.1% acetic acid; solution B consisted of acetonitrile, 0.1% FA, and 0.1% acetic acid; gradient, 0 to 100% B; flow rate, 50 μl/min). The control samples were additionally measured using an ammonium acetate (NH_4OAc) mobile-phase buffer (pH 5.0) with the same gradient (solution A, 5 mM NH_4OAc in water; solution B, 5 mM NH_4OAc in acetonitrile). To resolve some coeluting compounds, the control samples were run with a nanoflow capillary ultrahigh performance LC system (Nano Ultra 2D Plus; Eksigent, Dublin, CA) coupled to the same LTQ-Orbitrap XL mass spectrometer. These control samples (7 μl) were loaded for a period of 30 min, followed by 1 h of separation over the analytical capillary column (capillary, 75 μm by ca. 25 cm, packed with Magic AQ 3 μm C_{18} resin). Full-scan mass spectra were acquired in positive-ion mode (m/z = 153 to 1,500) with an experimental resolving power (R) of 60,000 (m/z = 400). MS/MS spectra were simultaneously acquired using collision-induced dissociation (CID) in the Orbitrap using a parent ion intensity threshold of >10,000 and targeting the three most abundant species in the full-scan spectrum or selectively only predefined species on a parent ion list.

(iii) Data processing and analysis. For a schematic representation of the LC-MS analysis workflow, see Fig. 1. The HR-LC-MS data set was filtered for the characteristic ^{54}Fe-^{56}Fe isotope pattern that is associated with Fe complexes using the software ChelomEx (18). The desired Fe complexes (e.g., $[M\text{-}2H^+ + Fe^{3+}]^+$ or $[M\text{-}H^+ + Fe^{2+}]^+$) coeluted with species that had m/z values corresponding to the free siderophore (MH^+) and were present at intensities about 100 to 1,000 times higher than the Fe complex. To achieve high sensitivity in the detection of Fe chelates, we applied a filter that required the presence of at least 1 matched isotope pattern ($\Delta m/z$ ^{54}Fe-^{56}Fe = −1.9953 ± [0.0015 + 2 ppm], relative intensity ^{54}Fe/^{56}Fe = 0.064 [0.03 to 0.09]) around the apex of the peak and coelution of the Fe complex with the free ligand [for Fe(III), $\Delta m/z$ = −53.91928 ± (0.0015 + 2 ppm); for Fe(II), $\Delta m/z$ = −52.91145 ± (0.0015 + 2 ppm)]. To collect MS/MS spectra of possible siderophores, a parent ion list was generated using an extended list of possible siderophores by including also species that may not have shown an identified Fe isotope pattern because the ^{54}Fe intensity was below the detection limit but still showed coelution with species corresponding to the possible free ligand, whereby the intensity of the free ligand had to exceed that of the Fe complex more than 5-fold. The results were examined manually, and the free ligands of all species discovered as possible siderophores were included in the parent ion list for high-resolution MS/MS data acquisition in replicate runs. In further analyses, only those species were considered that were present in three replicate runs and also in biological replicate controls, extracted under exclusion of oxygen in the glove box, but not in the blank medium extract. Most known siderophores fall into a mass range between 400 and 1,500 atomic mass units (amu) (23). While we observed several unknown Fe chelators with molecular masses of <400 amu, they formed Fe complexes with two or more ligands and included also apparent mixed-ligand complexes. The binding of these species is less specific than those of true siderophores, and they may include, for example, fatty acids or amino acids. For this reason, we excluded species with molecular masses of <400 amu from further analysis.

MS/MS molecular networks. MS/MS spectra with the same parent ion mass (±5 ppm or 0.0025 amu) were averaged and denoised, and the ^{13}C isotopes were removed. All species selected for calculation of the network had significantly different retention times. Coeluting species were manually examined, and possible adducts (e.g., Na or K adducts), dimers, or apparent in-source fragmentation products were removed. The network was then generated by modification of methods previously described by Dorrestein and coworkers to adapt to high-resolution MS/MS spectra (28–30). Briefly, cosine scores were calculated for pairwise aligned MS/MS spectra reflecting similarity whereby 1 and 0 indicate identical spectra and no similarity, respectively. Two MS/MS peaks were matched if they had the same high-resolution mass (±0.005 amu) or if their masses differ exactly by the mass difference of the two parent ions (±0.005 amu). Only fragments with an m/z difference of ≥50 to the parent ion were used so as to exclude unspecific losses (e.g., H_2O or NH_3) while including, for example, a loss of the lightest amino acid, alanine. A database of known siderophore structures assembled previously (23) was used to match the masses of molecules and their MS/MS fragments (±5 ppm or 0.005 amu) and to reconstruct MS/MS spectra.

Targeted siderophore quantification during growth. Targeted quantification of siderophores was performed on a single quadrupole LC-MS system (Agilent 6120) equipped with a UV-vis spectrometer, in single-ion monitoring (SIM) mode. Sample aliquots of 1 ml were taken throughout the growth, sterile filtered through 0.2-μm syringe filters, and stored at −20°C until analysis. Prior to analysis, the samples were acidified with 0.1% acetic acid and 0.1% FA. Without further purification (no solid-

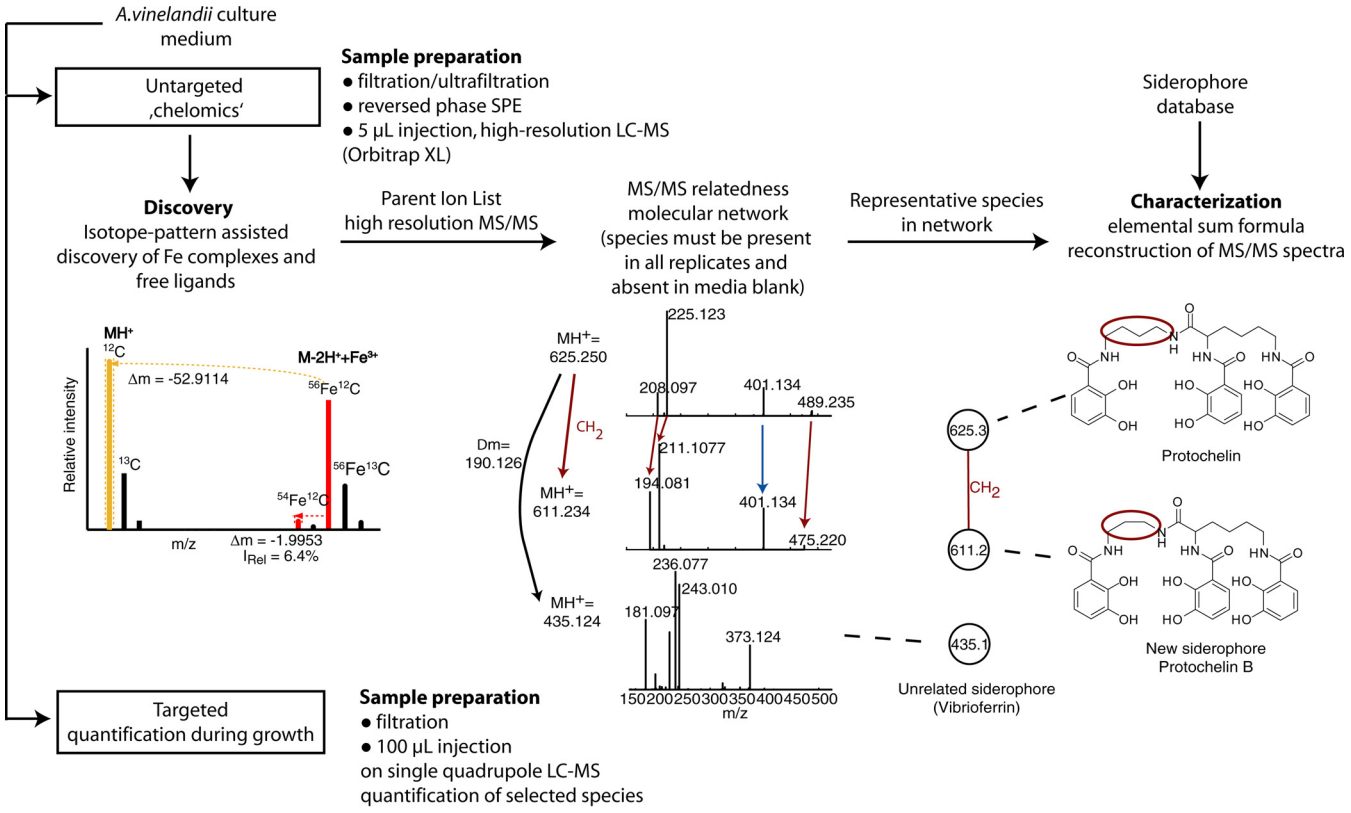

FIG 1 Schematic of the LC-MS analysis workflow in this study. For untargeted siderophore profiling ("chelomics"), sample preparation and measurement on a high-resolution LC-MS system were followed by mining of the LC-MS data for characteristic Fe isotope patterns associated with Fe complexes and the presence of associated Fe-free ligand species using ChelomEx software (18). MS/MS molecular networks of identified putative free siderophores were created to group structurally related species and assign mass differences between related species to sum formula differences. Identification of new siderophores was assisted by comparison of molecule and fragment masses to a database of known siderophore structures. Finally, manual reconstruction of MS/MS spectra allowed the assignment of chemical structures to several new siderophore structures. In some cases, the structure assignment was informed by additional NMR spectra of isolated compounds. Quantification of identified siderophores was performed on a single quadrupole LC-MS by direct injection of filtered spent media without prior solid-phase extraction (SPE).

phase extraction), 100-µl sample aliquots were injected onto a C_{18} column (Agilent Eclipse Plus C_{18} 3.5 µm, 4.6 by 100 mm) equipped with a matching guard column. The separation proceeded with the same mobile-phase system as the one described above for HR-LC-MS analyses (solution A, water–0.1% FA–0.1% acetic acid; solution B, acetonitrile–0.1% FA–0.1% acetic acid) over 30 min, at a flow rate of 0.8 ml/min. Using a 6-port valve, the column outflow was diverted to waste for the first 5.25 min, ensuring that the sample was completely desalted before introduction into the mass spectrometer. For quantification, LC-MS and UV-vis peak areas were determined using MassHunter software (Agilent). Relative elution times of the peaks on this system were matched to the elution times for the siderophores determined on the HR-LC-MS system. Peak areas were converted to concentrations by calibration with isolated standards of vibrioferrin, 2,3-dihydroxybenzoic acid (DHBA), azotochelin, protochelin, and azotobactin δ. The concentrations of minor derivatives were estimated using the LC-MS response determined for the structurally closely related major siderophores. Seven technical replicates of a spent medium "standard" collected in the stationary phase from a culture grown under the same conditions as the samples used for HR-LC-MS analysis (100 µM EDTA and 0.1 µM $FeCl_3$) showed relative standard deviations of <3.5% for the vibrioferrins and the major catechol siderophores. The remaining siderophores were measured with slightly larger standard deviations (<10% for siderophore concentrations above 0.5 µM and <20% for lower concentrations).

Siderophore isolation and quantification. Isolation of siderophores was achieved by filtration and solid-phase extraction (Oasis MAX or Oasis HLB) of culture media followed by HPLC purification with a C_{18} column. The pooled fractions were lyophilized and reconstituted with D_2O (vibrioferrin, aminochelin) or deuterated MeOH to obtain ^{1}H-NMR and correlation spectroscopy (COSY) spectra (Bruker Avance III 500MHz). Quantification of the isolated siderophore standards was performed by ^{1}H-NMR with internal standard addition of sodium benzoate for vibrioferrin or by UV-vis using reported extinction coefficients for acidified solutions of DHBA, aminochelin, azotochelin, protochelin, and azotobactin (5, 31).

RESULTS

Bioinformatic analyses of the *A. vinelandii* siderophore metabolome. We began by mining the genome of *A. vinelandii* strain CA (also known as OP; GenBank accession number CP005094.1) for siderophore biosynthetic genes and found a total of 9 NRPS genes and 2 NRPS-independent siderophore synthetase genes arranged across 5 clusters (Fig. 2; see also Table S1 in the supplemental material). Two of these clusters (AvCA_21160 to AvCA_21230 and AvCA_25530 to AvCA_25660) contain NRPS genes previously shown to be necessary for the production of catechols and azotobactin (24). Closer analysis of AvCA_09300 to AvCA_09360, one of the three new gene clusters, indicated that it possibly encodes the synthesis of a vibrioferrin-like compound, an α-hydroxycarboxylate siderophore characteristic of marine bacteria

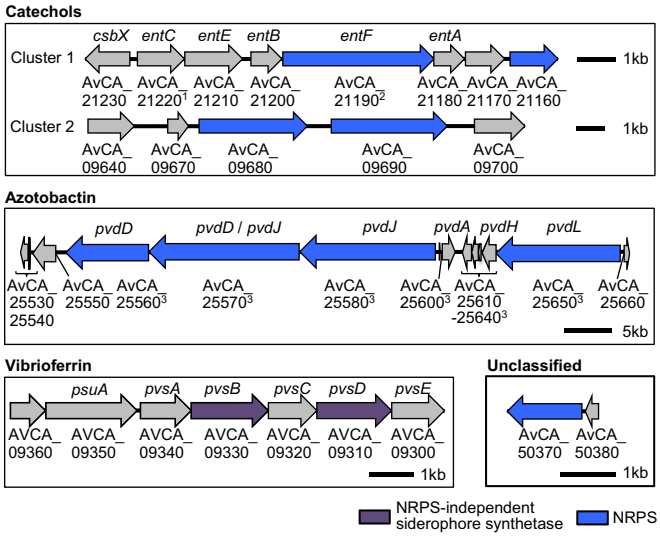

FIG 2 Nonribosomal peptide synthetase (NRPS) and NRPS-independent gene clusters in *A. vinelandii* strain CA (GenBank accession number CP005094.1). Genes necessary for production of specific siderophores are indicated by superscripts: superscript 1 indicates catechols (24); superscript 2 indicates catechols (25); superscript 3 indicates azotobactin (25). Annotated functions of genes as well as a more complete list of azotobactin-related biosynthetic genes can be found in Table S1 in the supplemental material.

such as *Vibrio parahaemolyticus* (32). Bioinformatics-based predictions of the specific siderophores produced by AvCA_09680 and AvCA_09690 are less clear; however, homology searches and the domain structure of these NRPS genes hint at an involvement in the later stages of protochelin biosynthesis (see below). The product of the last gene cluster, containing an MbtH-encoding gene (AvCA_50380) and an NRPS possessing only a single domain (AvCA_50370), is not known.

Discovery of unknown siderophores from *A. vinelandii*. To examine the product(s) of the *A. vinelandii* siderophore metabolome, we cultured *A. vinelandii* strain CA under diazotrophic and Fe-limited conditions, which have previously been shown to stimulate siderophore production (8). Initial mining of the HPLC-MS data for the ^{54}Fe-^{56}Fe isotope pattern associated with Fe(III) or Fe(II) siderophore complexes ($[M\text{-}2H^+ + Fe^{3+}]^+$ or $[M\text{-}H^+ + Fe^{2+}]^+$) and their related free ligands (MH^+) according to the scheme described in Fig. 1 revealed all previously known siderophores (shown in green in Fig. 3), but also a large number of other possible Fe-chelating agents. The Fe complexes of all species coeluted with their corresponding apo ligands, which were significantly more abundant than the Fe complexes as expected from the acidic (pH ~2.5) and low-Fe conditions used for chromatography.

Among the most abundant Fe chelators were species that matched the *m/z* values of the known siderophores produced by *A. vinelandii* CA, i.e., the fluorescent siderophores azotobactin D and azotobactin δ, as well as the catechol siderophores aminochelin, azotochelin, and protochelin (in green in Fig. 3). The identity of these known siderophores was further established by their MS/MS fragmentation patterns (see Fig. S1 in the supplemental material). Moreover, we found a large number of high-abundance Fe chelators with as-of-yet unassigned structures. Together, over 35 siderophores were reproducibly found in three biological replicates.

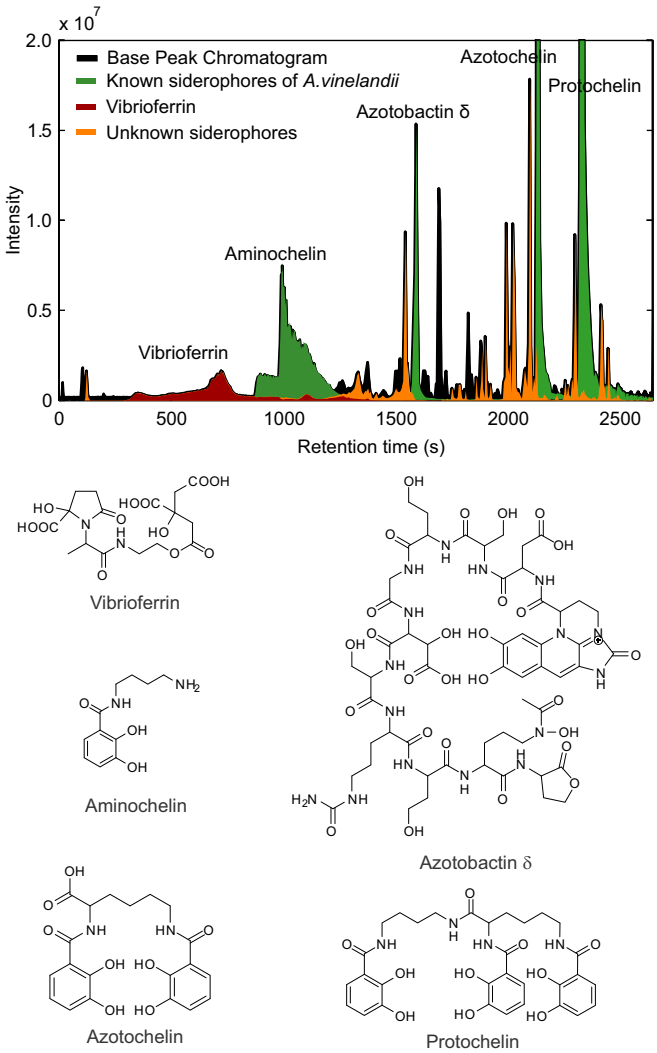

FIG 3 Base peak chromatogram (BPC) for the high-resolution LC-MS analysis of the *A. vinelandii* spent medium (black). Overlying the BPC are extracted ion chromatograms of the known siderophores from *A. vinelandii* (green). Siderophores that have not been reported before from *A. vinelandii* include the hydrophilic vibrioferrin (red) and a large number of new siderophores (orange), which were found to be related to the known siderophores produced by the bacterium.

These include hydrophilic siderophores, previously not reported in *A. vinelandii* (shown in red in Fig. 2), as well as new derivatives of old siderophores (shown in orange in Fig. 3).

Siderophore molecular networks: identification of vibrioferrins, azotobactins, and catechol siderophores. To obtain an overview of the structural similarity and diversity among *A. vinelandii* siderophores, we collected HR-MS/MS data for each compound and created a spectral network, an approach recently pioneered by the Dorrestein group (29). In this network, each node represents an individual siderophore (adducts, dimers, etc., were manually removed), while lines connecting the nodes represent commonalities in MS/MS fragmentation (Fig. 4A). The network revealed three groups of compounds structurally related to azotobactins, catechol siderophores, and vibrioferrin, a siderophore previously not observed in *A. vinelandii*.

Vibrioferrin cluster. The most prominent peak in the vibrio-

ferrin group of compounds was a hydrophilic Fe chelator that had the same mass as the siderophore vibrioferrin (33), which has previously been detected only in marine bacteria ($m/z = 435.125$) (Fig. 4B). Purification of this siderophore and subsequent analysis by MS/MS and NMR (^{1}H-NMR and COSY) confirmed its identity (see Fig. S2 in the supplemental material). This assignment is consistent with bioinformatic analysis of the *A. vinelandii* genome, which reveals a conserved *pvs* gene cluster (AvCA_09300 to AvCA_09360), responsible for vibrioferrin biosynthesis in *V. parahaemolyticus* (34) (Fig. 2; see also Fig. S2 in the supplemental material). Vibrioferrin is likely assembled from citrate, Ala, ethanolamine (derived from Ser), and α-ketoglutarate (35). We identified two new derivatives, one where the Ala precursor was replaced with Ser (vibrioferrin B), and another bearing a methyl ester within the citrate substructure (vibrioferrin C). The structural assignment of these analogs is based on HR-MS/MS data and on isotopic feeding experiments with L-[3,3,3-$^2H_3$]Ala, which resulted in a 3-Da mass shift with vibrioferrins A and C, but not B, consistent with the structures shown in Fig. 4B (see Fig. S3 in the supplemental material). These new derivatives are consistent with precursor flexibility and post-synthetic tailoring in the vibrioferrin biosynthetic pathway.

Catechol cluster. In addition to the known catechol siderophores, the HR-LC-MS data revealed a number of derivatives that differed by simple chemical modifications (±O; ±2H; CH_2 groups). Larger differences corresponded to addition or loss of a dihydroxybenzoyl group ($C_7H_4O_3$, $\Delta m = 136.013$) or an aminochelin group ($C_{11}H_{14}O_3N_2$, $\Delta m = 222.100$), the building blocks of azotochelin and protochelin. Based on MS/MS data, structures could be assigned to several noteworthy derivatives of protochelin, which we denote protochelin B through G (Fig. 4C; see also Fig. S4 to S6 in the supplemental material). For protochelin B, we detected a mass difference ($\Delta m/z$) of 14.016 relative to protochelin A for both the parent ion and some of its fragments, indicative of a loss of CH_2. Manual analysis of the MS/MS data revealed that the modification was located in the CH_2 chain of the aminochelin residue in protochelin as indicated by red circles in Fig. 4C (see also Fig. S4A in the supplemental material). Protochelins C to E, with m/z of 489.234, were assigned as analogs without a dihydroxybenzoyl group (DHB) (see Fig. S4B in the supplemental material). Three chromatographic peaks, each associated with different MS/MS fragmentation patterns, corresponded to the three structural isomers in which the DHB is missing in each of the three possible positions of protochelin. One of these analogs, protochelin C, is shown in Fig. 4C. MS data for protochelin F showed that it lacked two hydrogens relative to protochelin A. UV-vis spectra showed peak absorbances at λ of 330 nm in protochelin and in protochelin F, indicating that the structural change in the new analogue was not associated with an extended π-electron system. Instead, the aromatic substitution pattern inferred from ^{1}H-NMR spectra showed that the new compound was characterized by cross-linked catechol rings in agreement with the MS/MS spectra (see Fig. S5 and S6 in the supplemental material). The structure for the most prominent peak, protochelin F, is shown in Fig. 4C. A similar compound, protochelin G, with a different aromatic substitution pattern, was also isolated (see Fig. S6 in the supplemental material).

Azotobactin cluster. In the azotobactin network, several prominent siderophores had a larger mass than the known azotobactins (azotobactin δ and azotobactin D). The structure of azotobactin δ (m/z for $[M + 2H]^{2+} = 697.261$, $z = 2$) is characterized by a dihydroxyquinoline chromophore and a peptide chain with a homoserine-lactone at the terminus of the peptide chain, which are marked in orange and green, respectively, in Fig. 4D. Azotobactin D (m/z for $[M + 2H]^{2+} = 706.266$) has the same structure as azotobactin δ, with a terminal homoserine instead of the homoserine-lactone. The masses of the newly identified azotobactin derivatives match the masses of putative azotobactin precursors, which are characterized by modifications of the chromophore with a glutamic acid side chain. These structures have been suggested to occur in the following oxidative cascade in pseudomonads: ferribactin → hydroxyl-ferribactin → dihydropyoverdine → pyoverdine → azotobactin (36–38) (Fig. 4D). Changes in the putative chromophore structures were also in agreement with expected shifts in the UV-vis spectra. The hydroxyl-ferribactin δ (m/z for $[M + 2H]^{2+} = 750.807$) was the most abundant azotobactin derivative in this study. All azotobactin derivatives in Fig. 4D had the same peptide chain as the previously known azotobactins and a structural change in the chromophore with an additional glutamic acid side chain. An exception is a compound with an additional CH_2 group (m/z for $[M + 2H]^{2+} = 713.274$), which we denote azotobactin D2. MS/MS spectra indicated that the additional CH_2 was located at the homoserine end of azotobactin D2, likely representing a methyl ester or methyl ether derivative of homoserine (in green in Fig. 4D).

Pyoverdines, siderophores produced by pseudomonads, chemically closely related to azotobactins, show a remarkable diversity in their peptide structures between species and strains (e.g., *Pseudomonas aeruginosa* [39]), which is encoded by the NRPS genes. Nonetheless, in the three closely related *A. vinelandii* strains that have been sequenced (DJ, CA, CA6) (1, 40), the NRPS genes are 100% identical.

Siderophore production during growth. Why does *A. vinelandii* simultaneously produce three structurally distinct groups of siderophores? We sought to answer this question by studying the effects of different Fe sources on siderophore production. *A. vinelandii* was cultured under diazotrophic conditions with four different sources of Fe: condition 1, 0.1 μM Fe with 100 μM EDTA, i.e., the same conditions used for HR-LC-MS siderophore discovery; condition 2, 5 μM Fe with 100 μM EDTA; condition 3, hematite; and condition 4, freshly precipitated amorphous Fe oxide. We quantified siderophores by direct injection on a quadrupole LC-MS without prior solid-phase extraction, thus avoiding possible analytical errors from low analyte recoveries or preconcentration artifacts.

Under conditions 2 and 4, the cells grew rapidly and reached high optical densities (OD) after 3 days, while slow growth and low maximum OD indicated severe Fe limitation under conditions 1 and 3 (Fig. 5). Vibrioferrin A was the major siderophore under all tested growth conditions, present at 4 to 14 times the concentration of any of the other siderophores (Fig. 5). Vibrioferrin A was detected at particularly high concentrations in the late exponential growth phase under condition 2 (high Fe with EDTA), reaching concentrations up to 360 μM. Vibrioferrin derivatives were present at ~10 times lower concentrations (vibrioferrin B, 3 to 11 μM; vibrioferrin C, 0 to 4 μM). The abundant production of vibrioferrins under condition 2 (high Fe with EDTA) was followed by a rapid production of aminochelin and azotochelin, which reached final concentrations of 60 and 75 μM, respectively. In contrast, when cells were grown with highly available amorphous Fe oxide, aminochelin and azotochelin concen-

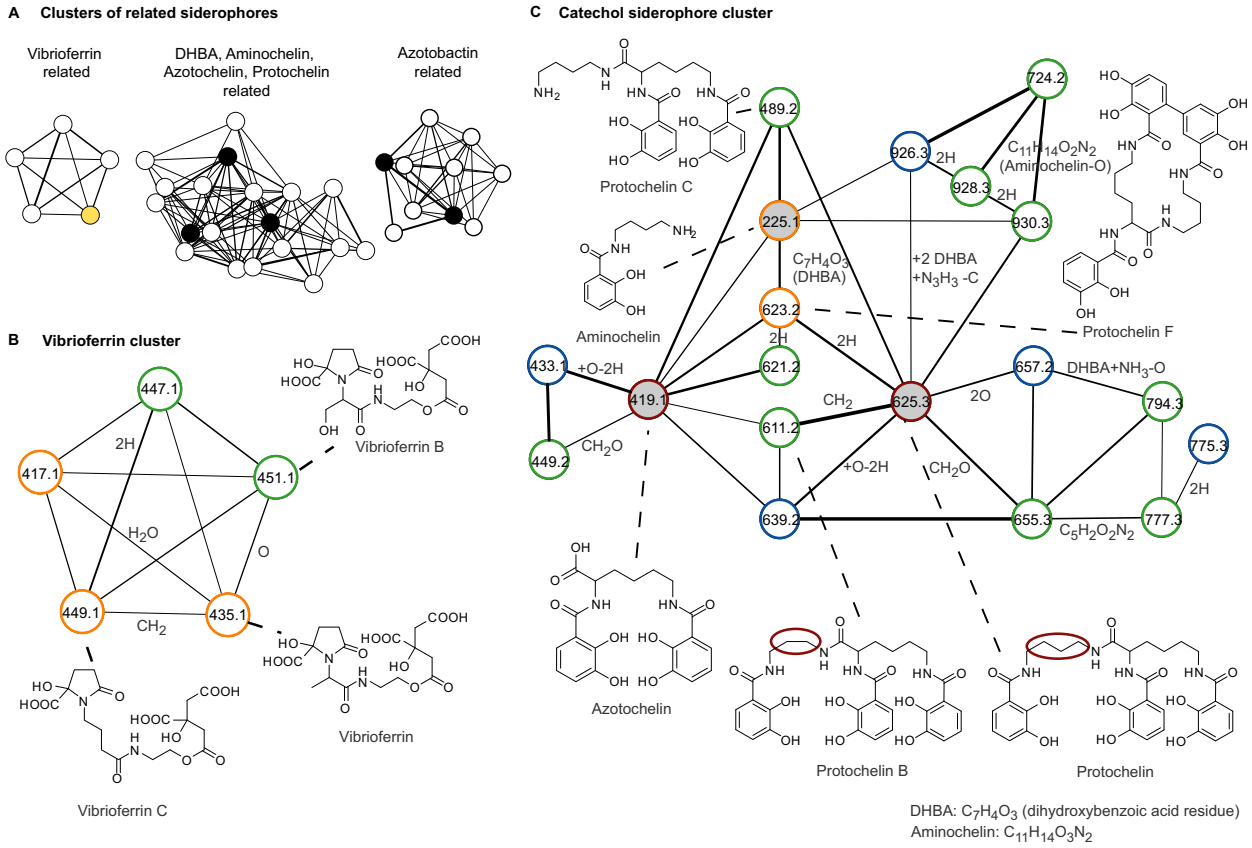

trations remained very low (<1.5 μM), while intermediate concentrations (7 to 10 μM) were reached under conditions of severe Fe limitation (added 0.1 μM Fe with 100 μM EDTA or added hematite). Interestingly, the production of protochelin was remarkably insensitive to the Fe source, possibly due to its role as a metallophore for Mo (8), which was added at a concentration close to the observed maximum protochelin concentrations in all treatments ([Mo] = 1 μM). The most abundant protochelin derivative, protochelin D, was found at concentrations similar to those of protochelin A (~1 μM), but it was not formed under condition 4. Azotobactins and related compounds were observed only under severe Fe limitation (conditions 1 and 3), in agreement with previous observations (4, 41). Azotobactins D and δ reached concentrations of <1 μM. The newly identified azotobactin-related siderophores hydroxyl-ferribactin δ and hydroxyl-ferribactin D were present at concentrations of up to 2 μM. The hydroxyl-ferribactins were detected at higher concentrations than the azotobactins under condition 3 (hematite) but at lower concentrations under condition 1 (low Fe with EDTA).

The relative timings of production of each siderophore were roughly similar under all conditions: (i) protochelin synthesis occurred during the initial lag and early growth phase, (ii) massive vibrioferrin production occurred after an initial fast growth phase, and (iii) production of aminochelin, azotochelin, and the known azotobactins occurred starting late in the initial rapid growth phase and continuing in the later growth phase. The major azotobactin derivatives, hydroxyl-ferribactin δ and hydroxyl-ferribactin D, increased earlier than the known azotobactins. Production of vibrioferrins B and C followed that of vibrioferrin A, while the protochelin derivatives peaked later than protochelin A. These results provide some clues regarding the role of each siderophore and have implications for the ability of bacteria to synthesize numerous siderophores, as discussed below.

DISCUSSION

Complete descriptions of siderophore metabolomes are a necessary precondition to address successfully the important and outstanding question of why microorganisms produce simultaneously a large set of distinct siderophores and why this set is different in different species. By exploiting state-of-the-art HR-LC-MS analysis combined with new data processing techniques, this study provides the most complete analysis to date of siderophores produced by any microorganism. Aside from the previously known azotobactins and catechol siderophores, we have identified the presence of additional, abundant, and previously unreported siderophores produced by *A. vinelandii*, including the hydrophilic vibrioferrin and its derivatives as well as analogs of azotobactin, azotochelin, protochelin, and aminochelin (see Table S2 in the supplemental material). These findings raise questions regarding the biosynthetic origins and possible functions of the new siderophores.

Vibrioferrin production by *A. vinelandii* and other bacteria. Vibrioferrin is the siderophore produced at the highest concentration under all tested conditions (diazotrophic growth with various sources and availabilities of Fe), even though it has not been detected previously in the *A. vinelandii* growth medium (Fig. 5). One possible explanation is that vibrioferrin is more hydrophilic than the previously known *A. vinelandii* siderophores and might not be retained by some reversed-phase extraction protocols. Vibrioferrin production was first observed in *V. parahaemolyticus* and since then has been found in several marine bacteria, including *Marinobacter* symbionts of dinoflagellates (42, 43). Our study provides an example of vibrioferrin production outside the marine environment. Genomic analysis for *pvs* genes, previously shown to be responsible for vibrioferrin biosynthesis (32), reveals striking conservation of the *pvsABCDE* gene cluster in bacteria from multiple phyla, environments, and lifestyles (Fig. 6). These genes are found primarily in *Gammaproteobacteria*, including several nonmarine organisms that are free-living or pathogenic. Thus, the potential for vibrioferrin production is more widespread than previously recognized. Additionally, the presence of *pvs* genes on a plasmid of *Ralstonia eutropha*, a betaproteobacterium, suggests that bacterial conjugation may be a mechanism for horizontal transfer of vibrioferrin genes.

In *A. vinelandii*, vibrioferrin production was particularly pronounced during the late exponential-growth phase in media with high initial added Fe (5 μM) and an excess of EDTA (100 μM) (condition 2 [Fig. 5]). Under the same condition, we also observed the highest concentrations of aminochelin and azotochelin. This strong coproduction of vibrioferrin, aminochelin, and azotochelin during the late exponential phase likely reflected the low concentrations of available Fe related to the slow dissociation of the Fe-EDTA complex, which cannot keep up with the demands of the multiplying bacterium (44, 45). Our finding of abundant vibrioferrin production outside a marine environment and without light indicates that Fe is made available to bacteria via mechanisms other than the previously suggested photoreduction of Fe-vibrioferrin (42, 43). Vibrioferrin is hydrophilic and a weak Fe chelator (pFe = $-\log [Fe^{3+}]$ = 18.4 with [vibrioferrin] = 10^{-5} M, [Fe] = 10^{-6} M, pH 7.4) (43). The strong coproduction of the weak, hydrophilic, and concentrated vibrioferrin with the stronger, more hydrophobic, and less concentrated azotochelin (pFe = 23.1 [31]) may be

FIG 4 (A) MS/MS molecular network of siderophores produced by *A. vinelandii*. Each node represents a separate siderophore (adducts, dimers, etc., have been removed) that was required to be present in biological and analytical replicates. The thickness of the edge represents the degree of relatedness between the MS/MS spectra of two species. The known siderophores from *A. vinelandii* are indicated as black circles, and vibrioferrin is indicated as a yellow circle. Three separate clusters can be recognized and include vibrioferrin, catechol siderophores, and azotobactins. The software Cytoscape was used for visualization. (B, C, D) Nodes in the three clusters shown in more detail. For these networks, nodes were manually arranged, and only selected edges are shown for clarity of presentation. The ring color around the nodes represents the peak area for each species, and the number represents the corresponding *m/z* value (rounded to one digit). The exact mass difference between two nodes was assigned to chemical sum formulas as indicated. Structures of new siderophores are based on reconstruction of MS/MS spectra and additional UV-vis and NMR spectroscopic data (see the text). The table in panel D shows the MS/MS fragmentation of azotobactin-related compounds. Arrows indicate MS/MS fragments corresponding to the B (arrows to the left) and Y (arrows to the right) fragment ions; λ_{max} is the absorption maximum of each compound in the UV-vis spectrum. Note that all siderophore species in the azotobactin cluster were doubly charged. ChrA, azotobactin chromophore; Febn, ferribactin; OHFebn, hydroxyl-ferribactin; ChrP, pyoverdine chromophore; 2HChrP, dihydropyoverdine; Ser, serine; Glu, glutamate; Hse, homoserine; Gly, glycine; OHAsp, hydroxyl aspartate; Cit, citrulline; AcOHOrn, acylhydroxyornithine; Hsl, homoserine lactone; MeHse, methylhomoserine; nd, not determined.

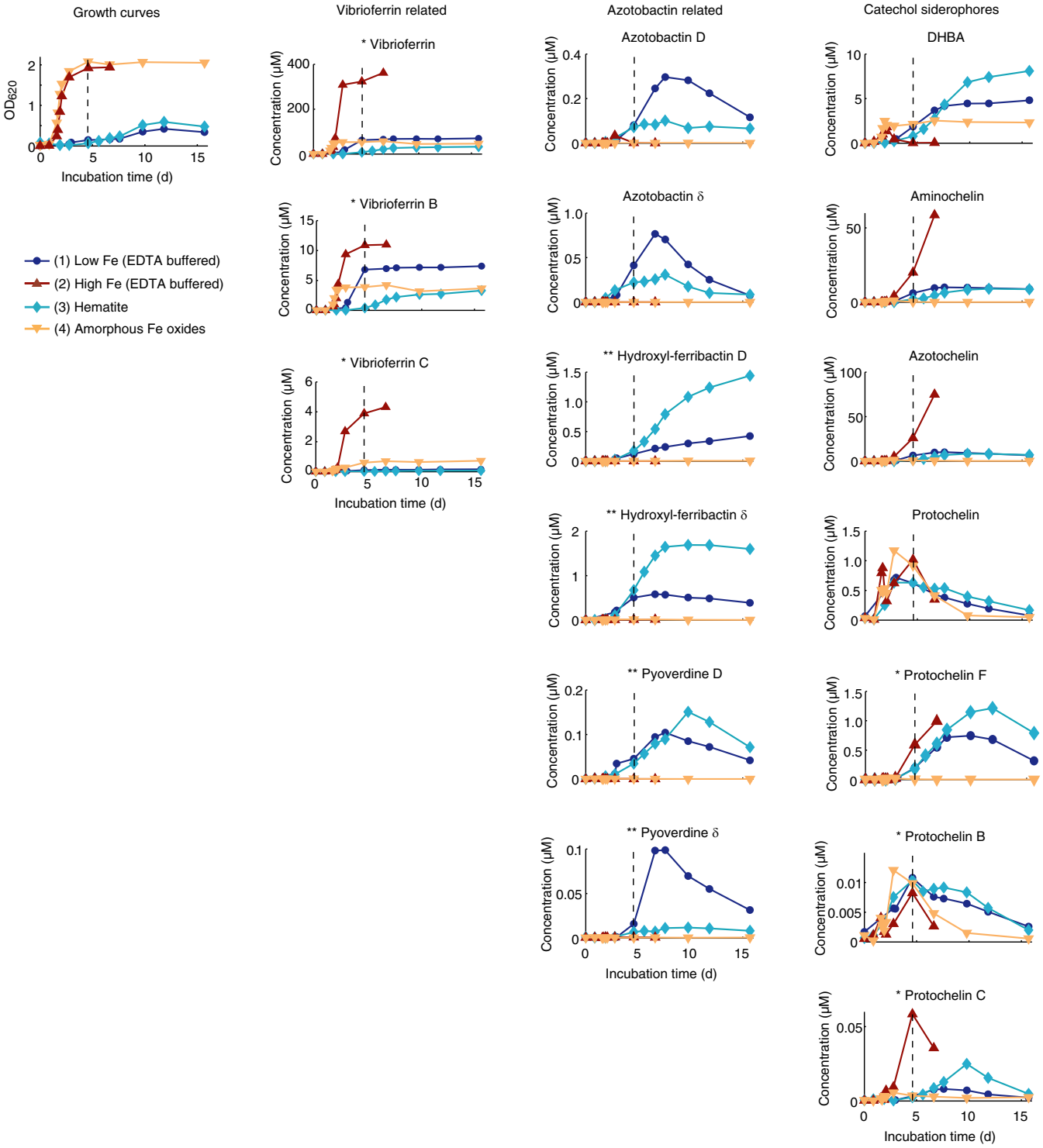

FIG 5 Concentration of notable siderophores from *A. vinelandii* under diazotrophic growth with different sources and availability of Fe. Growth was monitored by optical density at 620 nm (OD_{620}). * and ** indicate new *A. vinelandii* siderophores identified in this study. Double asterisks represent azotobactin derivatives based on MS/MS fragmentation patterns as shown in Fig. 3. Relative standard deviations were <3.5% for the vibrioferrins and the major catechol siderophores based on replicate analyses of a representative spent medium "standard." The remaining siderophores were measured with slightly larger standard deviations (<10% for siderophore concentrations above 0.5 μM and <20% for lower concentrations).

required in a "bucket brigade" mechanism that involves binding of Fe by vibrioferrin in the bulk medium and exchange with a hydrophobic siderophore that delivers Fe to the cell (46, 47). As such, the disparate siderophores would act synergistically in the acquisition of Fe (48). Notably, several bacteria with vibrioferrin biosynthetic genes (shown in Fig. 6) can potentially also produce other, structurally unrelated siderophores, which may be used in a bucket brigade mechanism.

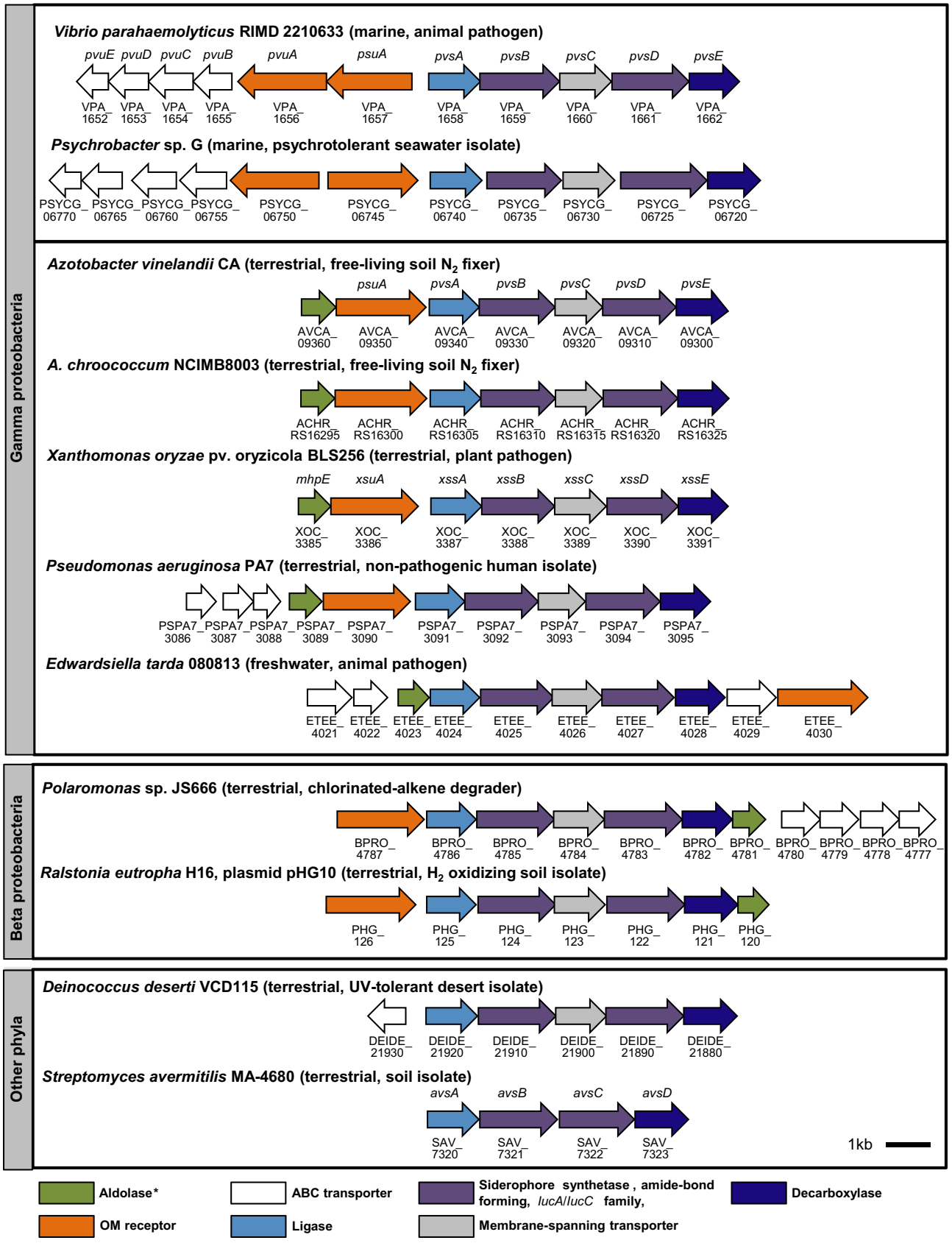

FIG 6 Occurrence of vibrioferrin biosynthetic genes (*pvs*) in bacteria from diverse phyla, environments, and lifestyles. Information on gene loci is displayed below each arrow. GenBank accession numbers for genomes shown (in order) are BA000032.2, CP006265.1, CP005094.1, CP010415.1, CP003057.1, CP000744.1, CP006664.1, CP000316.1, AY305378.1, CP001114.1, and BA000030.3. *, aldolase has been shown to be citrate synthase in *Staphylococcus* production of staphyloferrin B (60).

When grown with amorphous Fe oxide (condition 4), *A. vinelandii* grows as fast, and reaches the same OD, as with high Fe and EDTA (condition 2), but the siderophore pool consists almost exclusively of vibrioferrin and DHBA, with aminochelin and azotochelin at very low levels. Notably, both vibrioferrin (pK_a values of 5.1, 3.6, and 2.7 [43]) and DHBA (pK_a = 2.9) are negatively charged at the experimental pH (pH 6.9), unlike aminochelin (pK_a values of 7.1, 10.2, and 12.1 [49]), the other hydrophilic siderophore of *A. vinelandii*, which is positively charged. The negative charge of vibrioferrin and DHBA favors adsorption on positively charged Fe-oxyhydroxides (at pH <8), which may help in the dissolution of Fe and explain their elevated production compared to that of all other siderophores under condition 4. Thus, it appears that *A. vinelandii* can tailor its siderophore metabolome to existing sources of Fe in the environment.

Siderophore derivatives: artifacts, spontaneous reactions, or biosynthesis? The LC-MS analysis reveals new structural variations for vibrioferrin and the previously described *A. vinelandii* siderophores (Fig. 3 to 5). These related species were present at lower concentrations and may principally result from methodological artifacts, spontaneous reactions, or targeted biosynthesis. Methodological artifacts may potentially occur during sample preparation or LC-MS measurements, including (i) inadvertent oxidation, (ii) reactions due to acidification, (iii) reactions during the reversed-phase extraction, and (iv) reactions during ionization. To rule out oxidation or acidification, we performed control experiments in the absence of oxygen and at pH 5 instead of pH 2.5 by omitting sample acidification during solid-phase extraction and by using an ammonium acetate buffer (pH ~5) during LC-MS. All the derivatives shown in Fig. 4 were observed under anoxic conditions and at the higher pH, except for azotobactins and their derivatives, which were not retained on the solid-phase column or did not ionize at pH 5. The possibility of new species being caused by reversed-phase extraction is ruled out by the observation of many of the same derivatives via direct injection of the filtered medium into the LC-MS. Finally, species caused by reactions during the electrospray ionization process should coelute in the LC-MS chromatogram. Yet we observed separated chromatographic peaks for the siderophores shown in Fig. 4 (see also Table S2 in the supplemental material). Thus, potential methodological artifacts could clearly not explain the observed derivatives of the major *A. vinelandii* siderophores, and these are generated by spontaneous reactions or in an enzyme-dependent, "deliberate" fashion by the bacteria.

Derivatives of the catechol siderophores: biosynthesis and spontaneous reactions. The group of catechol siderophores is particularly diverse, and their biosyntheses have been well studied. We therefore bioinformatically investigated the production of the catechol siderophores. Analysis of the *ent* gene cluster, previously shown to be involved in catechol biosynthesis (cluster 1, AvCA_21180 to AvCA_21230 [Fig. 7A]), suggests that additional genes are required for production of aminochelin and protochelin (24, 25). This cluster can account for production of an EntB-bound DHB-thioester (Fig. 7B). Production of aminochelin from this intermediate requires incorporation of butane-1,4-diamine (putrescine), a reaction analogous to that catalyzed by VibH, an amide synthase from *Vibrio cholerae* that combines the polyamine norspermidine with DHB-thioesters in vibriobactin biosynthesis (50). A closer examination indeed indicates the presence of a VibH-like enzyme, which has 41% similarity (21% identity) to the *V. cholerae* VibH adjacent to the *ent* gene cluster (AVCA_21160) (Fig. 7A). Thus, a model can be proposed for production of aminochelin A (Fig. 7B). In an analogous fashion, aminochelin B would be generated from the same EntB-bound DHB intermediate and propane-1,3-diamine (Fig. 7B, dashed line 1), similar to the biosynthesis of serratiochelins, which also utilizes propane-1,3-diamine (51). Both diamines are well known and among the dominant forms in bacteria (52, 53). Thus, a single VibH-like homolog may incorporate several polyamines, consistent with previous *in vitro* studies on VibH (50).

For the bioproduction of the bis-catachol azotochelin, we predict that the large NRPS encoded by *entF* (AvCA_21190) catalyzes condensation of a T-domain-bound Lys with the DHB-thioester (Fig. 7C). Subsequent release from the assembly line via the termination (TE) domain would furnish azotochelin. On the other hand, the biosynthesis of protochelins will likely require involvement of an NRPS encoded at a different genetic locus, possibly one or both NRPSs found in cluster 2 (Fig. 7A). Among these, AvCA_09680 is especially intriguing as it contains the domain architecture C*-A-T, where C* represents a modified C domain with an HHXXXDA signature motif (rather than the canonical HHXXXDG sequence). A similar "unusual" C domain has been shown to condense a diffusible N^1-(2,3-dihydroxybenzoyl)norspermidine group with T-domain-bound DHB-thioester in the biosynthesis of vibriobactin (54). We therefore propose that this unusual NRPS is involved in the production of protochelin and derivatives B, E, and C (Fig. 7C, dashed lines 2 to 4). In the case of protochelin B, aminochelin B is utilized as the diffusible substrate, whereas biosyntheses of protochelins A/C and E require aminochelin A and putrescine, respectively. Generation of these kinds of analogs, lacking a DHB moiety, was previously also observed for vibriobactins (55). Thus, biosynthetic origins can be proposed for many of the siderophore analogs using bioinformatic analyses.

Some species that we have detected may also be formed by spontaneous postsynthesis reactions. In particular, protochelin F may be derived from such a route for 3 reasons: (i) its structure is characterized by a direct intramolecular cross-link between two catechol rings hindering Fe binding; (ii) it has several isomers, such as protochelin G, with the link between the catechol rings at different positions arguing against a defined enzymatic synthesis; and (iii) its concentration peaks late during growth, when protochelin concentrations decrease (Fig. 5). A possible formation mechanism in aerobic *A. vinelandii* cultures involves oxidation of catechols to form cross-linked aromatic compounds, perhaps catalyzed by the presence of Fe (56, 57).

Functions of multiple siderophore derivatives. In this study, we observed a large number of previously unreported derivatives of all the siderophores of *A. vinelandii*. The production of several related siderophores by a single organism has been observed for ferrioxamines, agrobactins, desferrichromes, enterobactins, mycobactins, and pyoverdines (23). The high sensitivity of our LC-MS approach reveals that even with compounds for which previously only one structure was known, such as for vibrioferrin, azotochelin, or protochelin, there are a large number of less abundant derivatives, vastly expanding on the known variations. Our detailed comparison of metabolomic and genetic data for catechol biosynthesis reveals a flexible substrate range and nonlinear siderophore assembly as key mechanisms for generating chemical diversity. These reactions give rise to structural modifications with altered hydrophobicity, binding affinities, and kinetics of interac-

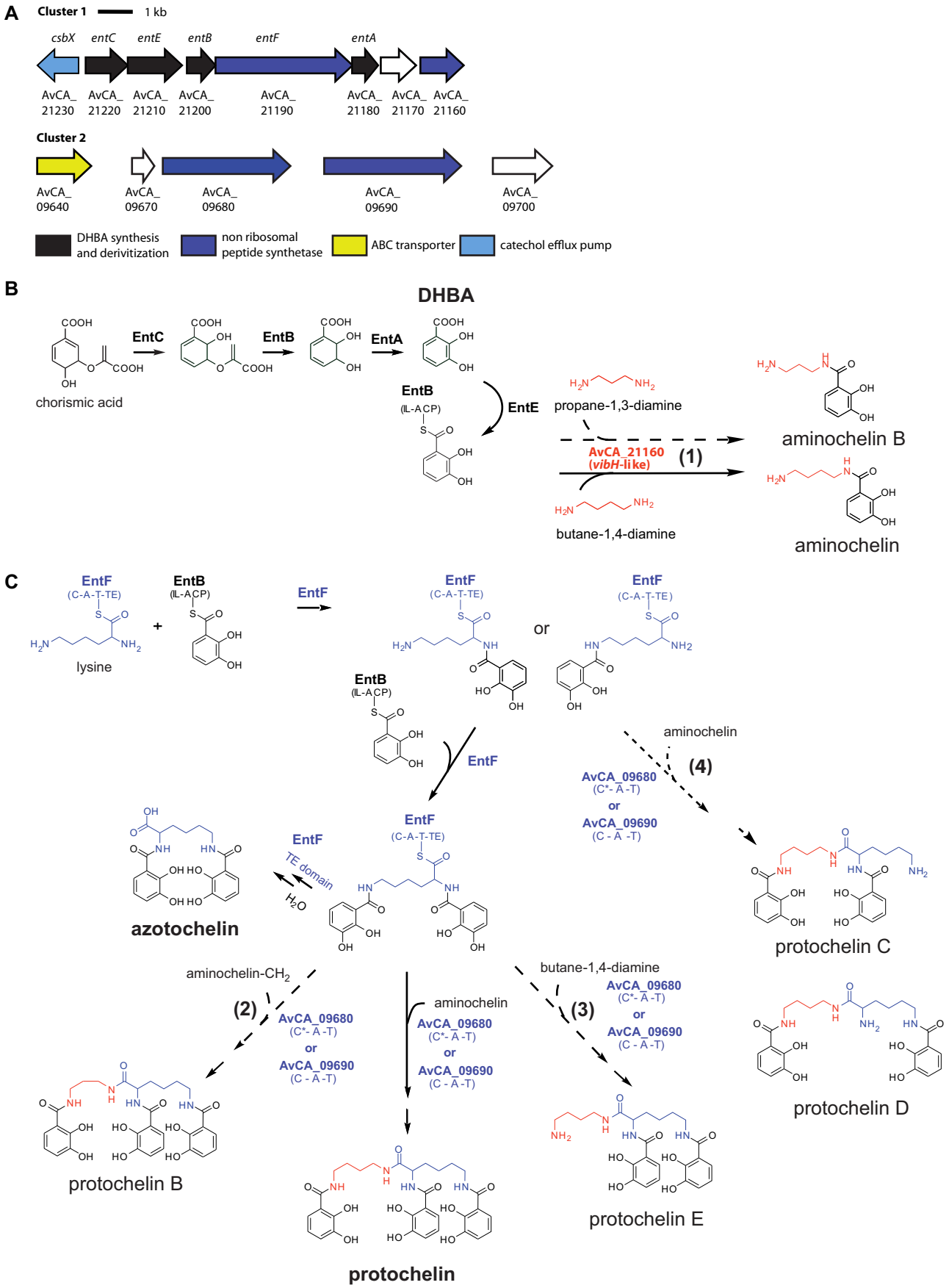

FIG 7 Proposed biosynthesis for *A. vinelandii* siderophores. (A) Mining of the *A. vinelandii* strain CA genome data suggests that two NRPS clusters are involved in catechol siderophore production. (B) Proposed biosynthesis pathway for monocatechol siderophores. (C) Proposed biosynthesis for bis- and tris-catechol siderophores. Bold text indicates previously characterized catechols. Dashed lines indicate pathways for derivatives identified in this study (Fig. 4).

tion with uptake transporters that natural selection may act upon during structurally mediated evolution of new siderophore functions.

Possible advantages of structural variation include the prevention of binding or uptake of siderophores by competing organisms. For example, it has been shown that streptomycetes produce additional siderophores when grown in coculture with competing strains (28). Structural variation of siderophores may also allow the organism to optimize uptake depending on environmental Fe chemistries (58), facilitate uptake of other required metals (e.g., Mo and V), or sequester toxic metals (e.g., W) (10). Siderophores may also act as redox shuttles, even as signaling molecules, and can serve multiple functions simultaneously (59). This leads to a fundamental reason for the vast structural variation: siderophore structures could result from multiple selective pressures that reflect evolutionary arms races including not just competition for low-abundance catalytic metals but also other processes. Future untargeted siderophore metabolomics analyses will further improve our understanding of conditions under which siderophores are produced and how these conditions relate to siderophore structural variations and function.

FUNDING INFORMATION

We thank the National Science Foundation (grant OCE 1315200 to F.M.M.M.), the Pew Biomedical Scholars Program (M.R.S.), and the Grand Challenge Program of the Princeton Environmental Institute (F.M.M.M., O.B., and M.R.S.) for financial support of this work.

REFERENCES

1. **Setubal JC, dos Santos P, Goldman BS, Ertesvag H, Espin G, Rubio LM, Valla S, Almeida NF, Balasubramanian D, Cromes L, Curatti L, Du ZJ, Godsy E, Goodner B, Hellner-Burris K, Hernandez JA, Houmiel K, Imperial J, Kennedy C, Larson TJ, Latreille P, Ligon LS, Lu J, Maerk M, Miller NM, Norton S, O'Carroll IP, Paulsen I, Raulfs EC, Roemer R, Rosser J, Segura D, Slater S, Stricklin SL, Studholme DJ, Sun J, Viana CJ, Wallin E, Wang BM, Wheeler C, Zhu HJ, Dean DR, Dixon R, Wood D.** 2009. Genome sequence of *Azotobacter vinelandii*, an obligate aerobe specialized to support diverse anaerobic metabolic processes. J Bacteriol **191:**4534–4545. http://dx.doi.org/10.1128/JB.00504-09.
2. **Wichard T, Mishra B, Myneni SCB, Bellenger JP, Kraepiel AML.** 2009. Storage and bioavailability of molybdenum in soils increased by organic matter complexation. Nat Geosci **2:**625–629. http://dx.doi.org/10.1038/ngeo589.
3. **Cornish A, Page W.** 1995. Production of the triacetecholate siderophore protochelin by *Azotobacter vinelandii*. Biometals **8:**332–338.
4. **Wichard T, Bellenger JP, Morel FMM, Kraepiel AML.** 2009. Role of the siderophore azotobactin in the bacterial acquisition of nitrogenase metal cofactors. Environ Sci Technol **43:**7218–7224. http://dx.doi.org/10.1021/es8037214.
5. **Palanche T, Blanc S, Hennard C, Abdallah MA, Albrecht-Gary AM.** 2004. Bacterial iron transport: coordination properties of azotobactin, the highly fluorescent siderophore of *Azotobacter vinelandii*. Inorg Chem **43:**1137–1152. http://dx.doi.org/10.1021/ic034862n.
6. **Hayat R, Ali S, Amara U, Khalid R, Ahmed I.** 2010. Soil beneficial bacteria and their role in plant growth promotion: a review. Ann Microbiol **60:**579–598. http://dx.doi.org/10.1007/s13213-010-0117-1.
7. **Seyedsayamdost MR, Traxler MF, Zheng S-L, Kolter R, Clardy J.** 2011. Structure and biosynthesis of amychelin, an unusual mixed-ligand siderophore from *Amycolatopsis sp*. AA4. J Am Chem Soc **133:**11434–11437. http://dx.doi.org/10.1021/ja203577e.
8. **Bellenger JP, Wichard T, Kustka AB, Kraepiel AML.** 2008. Uptake of molybdenum and vanadium by a nitrogen-fixing soil bacterium using siderophores. Nat Geosci **1:**243–246. http://dx.doi.org/10.1038/ngeo161.
9. **Huyer M, Page WJ.** 1988. Zn increases siderophore production in *Azotobacter vinelandii*. Appl Environ Microbiol **54:**2625–2631.
10. **Kraepiel AML, Bellenger JP, Wichard T, Morel FMM.** 2009. Multiple roles of siderophores in free-living nitrogen-fixing bacteria. Biometals **22:**573–581. http://dx.doi.org/10.1007/s10534-009-9222-7.
11. **Wichard T, Bellenger JP, Loison A, Kraepiel AML.** 2008. Catechol siderophores control tungsten uptake and toxicity in the nitrogen-fixing bacterium *Azotobacter vinelandii*. Environ Sci Technol **42:**2408–2413. http://dx.doi.org/10.1021/es702651f.
12. **Villa JA, Ray EE, Barney BM.** 2014. *Azotobacter vinelandii* siderophore can provide nitrogen to support the culture of the green algae *Neochloris oleoabundans* and *Scenedesmus sp*. BA032. FEMS Microbiol Lett **351:**70–77. http://dx.doi.org/10.1111/1574-6968.12347.
13. **Bulen WA, LeComte JR.** 1962. Isolation and properties of a yellow-green fluorescent peptide from Azotobacter medium. Biochem Biophys Res Commun **9:**523–528. http://dx.doi.org/10.1016/0006-291X(62)90119-5.
14. **Page WJ, Collinson SK, Demange P, Dell A, Abdallah M.** 1991. *Azotobacter vinelandii* strains of disparate origin produce azotobactin siderophores with identical structures. Biometals **4:**217–222.
15. **Corbin JL, Bulen WA.** 1969. Isolation and identification of 2,3-dihydroxybenzoic acid and N2,N6-di(2,3-dihydroxybenzoyl)-L-lysine formed by iron-deficient *Azotobacter vinelandii*. Biochemistry **8:**757–762. http://dx.doi.org/10.1021/bi00831a002.
16. **Page WJ, von Tigerstrom M.** 1988. Aminochelin, a catecholamine siderophore produced by *Azotobacter vinelandii*. J Gen Microbiol **134:**453–460.
17. **Smith AW.** 1998. Iron starvation and siderophore-mediated iron transport. Methods Microbiol **27:**331–342. http://dx.doi.org/10.1016/S0580-9517(08)70294-0.
18. **Baars O, Morel FMM, Perlman DH.** 2014. ChelomEx: isotope-assisted discovery of metal chelates in complex media using high-resolution LC-MS. Anal Chem **86:**11298–11305. http://dx.doi.org/10.1021/ac503000e.
19. **Lehner SM, Atanasova L, Neumann NKN, Krska R, Lemmens M, Druzhinina IS, Schuhmacher R.** 2013. Isotope-assisted screening for iron-containing metabolites reveals a high degree of diversity among known and unknown siderophores produced by *Trichoderma* spp. Appl Environ Microbiol **79:**18–31. http://dx.doi.org/10.1128/AEM.02339-12.
20. **Deicke M, Mohr JF, Bellenger J-P, Wichard T.** 2014. Metallophore mapping in complex matrices by metal isotope coded profiling of organic ligands. Analyst **139:**6096–6099. http://dx.doi.org/10.1039/C4AN01461H.
21. **Rosconi F, Davyt D, Martínez V, Martínez M, Abin-Carriquiry JA, Zane H, Butler A, de Souza EM, Fabiano E.** 2013. Identification and structural characterization of serobactins, a suite of lipopeptide siderophores produced by the grass endophyte *Herbaspirillum seropedicae*. Environ Microbiol **15:**916–927. http://dx.doi.org/10.1111/1462-2920.12075.
22. **Barry SM, Challis GL.** 2009. Recent advances in siderophore biosynthesis. Curr Opin Chem Biol **13:**205–215. http://dx.doi.org/10.1016/j.cbpa.2009.03.008.
23. **Hider RC, Kong XL.** 2010. Chemistry and biology of siderophores. Nat Prod Rep **27:**637–657. http://dx.doi.org/10.1039/b906679a.
24. **Yoneyama F, Yamamoto M, Hashimoto W, Murata K.** 2011. *Azotobacter vinelandii* gene clusters for two types of peptidic and catechol siderophores produced in response to molybdenum. J Appl Microbiol **111:**932–938. http://dx.doi.org/10.1111/j.1365-2672.2011.05109.x.
25. **Tindale AE, Mehrotra M, Ottem D, Page WJ.** 2000. Dual regulation of catecholate siderophore biosynthesis in *Azotobacter vinelandii* by iron and oxidative stress. Microbiology **146:**1617–1626. http://dx.doi.org/10.1099/00221287-146-7-1617.
26. **Blin K, Medema MH, Kazempour D, Fischbach MA, Breitling R, Takano E, Weber T.** 2013. antiSMASH 2.0—a versatile platform for genome mining of secondary metabolite producers. Nucleic Acids Res **41**(W1):W204–W212. http://dx.doi.org/10.1093/nar/gkt449.
27. **Overbeek R, Olson R, Pusch GD, Olsen GJ, Davis JJ, Disz T, Edwards RA, Gerdes S, Parrello B, Shukla M.** 2014. The SEED and the rapid annotation of microbial genomes using subsystems technology (RAST). Nucleic Acids Res **42:**D206–D214. http://dx.doi.org/10.1093/nar/gkt1226.
28. **Traxler MF, Watrous JD, Alexandrov T, Dorrestein PC, Kolter R.** 2013. Interspecies interactions stimulate diversification of the *Streptomyces coelicolor* secreted metabolome. mBio **4**(4):e00459-13. http://dx.doi.org/10.1128/mBio.00459-13.
29. **Watrous J, Roach P, Alexandrov T, Heath BS, Yang JY, Kersten RD, van der Voort M, Pogliano K, Gross H, Raaijmakers JM, Moore BS, Laskin J, Bandeira N, Dorrestein PC.** 2012. Mass spectral molecular networking of living microbial colonies. Proc Natl Acad Sci U S A **109:**E1743–E1752. http://dx.doi.org/10.1073/pnas.1203689109.
30. **Guthals A, Watrous JD, Dorrestein PC, Bandeira N.** 2012. The spectral

networks paradigm in high throughput mass spectrometry. Mol Biosyst **8:**2535–2544. http://dx.doi.org/10.1039/c2mb25085c.
31. **Cornish AS, Page WJ.** 1998. The catecholate siderophores of *Azotobacter vinelandii*: their affinity for iron and role in oxygen stress management. Microbiology **144:**1747–1754. http://dx.doi.org/10.1099/00221287-144-7-1747.
32. **Tanabe T, Funahashi T, Nakao H, Miyoshi S-I, Shinoda S, Yamamoto S.** 2003. Identification and characterization of genes required for biosynthesis and transport of the siderophore vibrioferrin in *Vibrio parahaemolyticus*. J Bacteriol **185:**6938–6949. http://dx.doi.org/10.1128/JB.185.23.6938-6949.2003.
33. **Yamamoto S, Okujo N, Yoshida T, Matsuura S, Shinoda S.** 1994. Structure and iron transport activity of vibrioferrin, a new siderophore of *Vibrio parahaemolyticus*. J Biochem **115:**868–874.
34. **Robson RL, Jones R, Robson RM, Schwartz A, Richardson TH.** 2015. Azotobacter genomes: the genome of *Azotobacter chroococcum* NCIMB 8003 (ATCC 4412). PLoS One **10:**e0127997. http://dx.doi.org/10.1371/journal.pone.0127997.
35. **Challis GL.** 2005. A widely distributed bacterial pathway for siderophore biosynthesis independent of nonribosomal peptide synthetases. ChemBioChem **6:**601–611. http://dx.doi.org/10.1002/cbic.200400283.
36. **Budzikiewicz H, Schäfer M, Fernández D, Matthijs S, Cornelis P.** 2007. Characterization of the chromophores of pyoverdins and related siderophores by electrospray tandem mass spectrometry. Biometals **20:**135–144. http://dx.doi.org/10.1007/s10534-006-9021-3.
37. **Taraz K, Tappe R, Schröder H, Hohlneicher U, Gwose I, Budzikiewicz H, Mohn G, Lefevre J.** 1991. Ferribactins—the biogenetic precursors of pyoverdins. Z Naturforsch **46:**527–533.
38. **Dorrestein PC, Poole K, Begley TP.** 2003. Formation of the chromophore of the pyoverdine siderophores by an oxidative cascade. Org Lett **5:**2215–2217. http://dx.doi.org/10.1021/ol034531e.
39. **Visca P, Imperi F, Lamont IL.** 2007. Pyoverdine siderophores: from biogenesis to biosignificance. Trends Microbiol **15:**22–30. http://dx.doi.org/10.1016/j.tim.2006.11.004.
40. **Noar JD, Bruno-Bárcena JM.** 2013. Complete genome sequences of *Azotobacter vinelandii* wild-type strain CA and tungsten-tolerant mutant strain CA6. Genome Announc **1**(3):e00313-13. http://dx.doi.org/10.1128/genomeA.00313-13.
41. **Page WJ, Huyer M.** 1984. Derepression of the *Azotobacter vinelandii* siderophore system, using iron-containing minerals to limit iron repletion. J Bacteriol **158:**496–502.
42. **Amin SA, Parker MS, Armbrust EV.** 2012. Interactions between diatoms and bacteria. Microbiol Mol Biol Rev **76:**667–684. http://dx.doi.org/10.1128/MMBR.00007-12.
43. **Amin SA, Green DH, Küpper FC, Carrano CJ.** 2009. Vibrioferrin, an unusual marine siderophore: iron binding, photochemistry, and biological implications. Inorg Chem **48:**11451–11458. http://dx.doi.org/10.1021/ic9016883.
44. **Shaked Y, Kustka AB, Morel FMM.** 2005. A general kinetic model for iron acquisition by eukaryotic phytoplankton. Limnol Oceanogr **50:**872–882. http://dx.doi.org/10.4319/lo.2005.50.3.0872.
45. **Sunda W, Huntsman S.** 2003. Effect of pH, light, and temperature on Fe-EDTA chelation and Fe hydrolysis in seawater. Mar Chem **84:**35–47. http://dx.doi.org/10.1016/S0304-4203(03)00101-4.
46. **Gobin J, Horwitz MA.** 1996. Exochelins of *Mycobacterium tuberculosis* remove iron from human iron-binding proteins and donate iron to mycobactins in the *M. tuberculosis* cell wall. J Exp Med **183:**1527–1532. http://dx.doi.org/10.1084/jem.183.4.1527.
47. **Martinez JS, Carter-Franklin JN, Mann EL, Martin JD, Haygood MG, Butler A.** 2003. Structure and membrane affinity of a suite of amphiphilic siderophores produced by a marine bacterium. Proc Natl Acad Sci U S A **100:**3754–3759. http://dx.doi.org/10.1073/pnas.0637444100.
48. **Challis GL, Hopwood DA.** 2003. Synergy and contingency as driving forces for the evolution of multiple secondary metabolite production by Streptomyces species. Proc Natl Acad Sci U S A **100:**14555–14561. http://dx.doi.org/10.1073/pnas.1934677100.
49. **Khodr H, Hider R, Duhme-Klair AK.** 2002. The iron-binding properties of aminochelin, the mono(catecholamide) siderophore of *Azotobacter vinelandii*. J Biol Inorg Chem **7:**891–896. http://dx.doi.org/10.1007/s00775-002-0375-x.
50. **Keating TA, Marshall CG, Walsh CT.** 2000. Vibriobactin biosynthesis in *Vibrio cholerae*: VibH is an amide synthase homologous to nonribosomal peptide synthetase condensation domains. Biochemistry **39:**15513–15521. http://dx.doi.org/10.1021/bi001651a.
51. **Seyedsayamdost MR, Cleto S, Carr G, Vlamakis H, João Vieira M, Kolter R, Clardy J.** 2012. Mixing and matching siderophore clusters: structure and biosynthesis of serratiochelins from *Serratia sp.* V4. J Am Chem Soc **134:**13550–13553. http://dx.doi.org/10.1021/ja304941d.
52. **Shah P, Swiatlo E.** 2008. A multifaceted role for polyamines in bacterial pathogens. Mol Microbiol **68:**4–16. http://dx.doi.org/10.1111/j.1365-2958.2008.06126.x.
53. **Lee J, Sperandio V, Frantz DE, Longgood J, Camilli A, Phillips MA, Michael AJ.** 2009. An alternative polyamine biosynthetic pathway is widespread in bacteria and essential for biofilm formation in *Vibrio cholerae*. J Biol Chem **284:**9899–9907. http://dx.doi.org/10.1074/jbc.M900110200.
54. **Marshall CG, Hillson NJ, Walsh CT.** 2002. Catalytic mapping of the vibriobactin biosynthetic enzyme VibF. Biochemistry **41:**244–250. http://dx.doi.org/10.1021/bi011852u.
55. **Keating TA, Marshall CG, Walsh CT.** 2000. Reconstitution and characterization of the Vibrio cholerae vibriobactin synthetase from VibB, VibE, VibF, and VibH. Biochemistry **39:**15522–15530. http://dx.doi.org/10.1021/bi0016523.
56. **Harrington JM, Bargar JR, Jarzecki AA, Roberts JG, Sombers LA, Duckworth OW.** 2012. Trace metal complexation by the triscatecholate siderophore protochelin: structure and stability. Biometals **25:**393–412. http://dx.doi.org/10.1007/s10534-011-9513-7.
57. **Devlin HR, Harris IJ.** 1984. Mechanism of the oxidation of aqueous phenol with dissolved oxygen. Ind Eng Chem Fundam **23:**387–392. http://dx.doi.org/10.1021/i100016a002.
58. **Wilson MK, Abergel RJ, Arceneaux JEL, Raymond KN, Byers BR.** 2010. Temporal production of the two *Bacillus anthracis* siderophores, petrobactin and bacillibactin. Biometals **23:**129–134. http://dx.doi.org/10.1007/s10534-009-9272-x.
59. **Adler C, Corbalán NS, Seyedsayamdost MR, Pomares MF, de Cristóbal RE, Clardy J, Kolter R, Vincent PA.** 2012. Catecholate siderophores protect bacteria from pyochelin toxicity. PLoS One **7:**e46754. http://dx.doi.org/10.1371/journal.pone.0046754.
60. **Cheung J, Murphy MEP, Heinrichs DE.** 2012. Discovery of an iron-regulated citrate synthase in *Staphylococcus aureus*. Chem Biol **19:**1568–1578. http://dx.doi.org/10.1016/j.chembiol.2012.10.003.